Received: 7 May 2017 | Accepted: 1 July 2017

DOI: 10.1111/jace.15077

ORIGINAL ARTICLE

Journal of the American Ceramic Society

Octahedral distortion, phase structural stability, and microwave dielectric properties in equivalently substituted $LaTiNbO_6$ ceramics

Jian Zhang | **Ruzhong Zuo**

Institute of Electro Ceramics & Devices, School of Materials Science and Engineering, Hefei University of Technology, Hefei, China

Correspondence
Ruzhong Zuo, Institute of Electro Ceramics & Devices, School of Materials Science and Engineering, Hefei University of Technology, Hefei, China.
Emails: rzzuo@hotmail.com; piezolab@hfut.edu.cn

Funding information
the Special Funds for Science and Technology Development of Guangdong Province, Grant/Award Number: 2017A010101001; Natural Science Foundation of Anhui Province, Grant/Award Number: 1508085JGD04

Abstract

The room-temperature phase composition, microstructural characteristic, and microwave dielectric properties of equivalently substituted $LaTiNbO_6$ ceramics were investigated by means of the Rietveld structural refinement, scanning electron microscopy, and network analyzer. A special interest was focused on the influence of the variation in bond length and octahedral distortion on the phase structural stability. A monoclinic (M) aeschynite phase was obtained in B-site ions (Ta^{5+} and $[W_{0.5}Ti_{0.5}]^{5+}$) substituted $LaTiNbO_6$ ceramics while an orthorhombic (O) aeschynite structure appeared in B-site ions (Zr^{4+}) or A-site ions (Ce^{3+} and Sm^{3+}) substituted $LaTiNbO_6$ ceramics, which owned typical polygonal and short rod-like grain morphologies, respectively. Compared with the octahedral bond length, a straightforward relation between the phase structural stability and the octahedral distortion was established, in which a reduced octahedral distortion was directly correlated with the destabilization of O or M phases or vice versa, irrespective of the substitution ionic radius. The experimentally observed giant difference in dielectric performance of $LaTiNbO_6$ based ceramics was believed to mainly originate from their distinct phase structure and grain morphology.

KEYWORDS
dielectric materials/properties, microstructure, phase transformations, X-ray methods

1 | INTRODUCTION

A series of $RETi(Nb,Ta)O_6$ (RE: rare-earth ions) materials with general formula AB_2O_6 has achieved broad attention for their great potentials in a variety of fields, such as mobile and satellite communication systems, miniature solid-state laser, and luminescence applications.[1-6] Their microwave dielectric properties were firstly reported by Sebastian and his co-workers.[4,5] With increasing A-site RE atomic number (Z), a morphotropic phase transformation from the orthorhombic (O) aeschynite (*Pnma* space group) to the O-type euxenite (*Pbcn* space group) appeared between Eu (Z=63) and Gd (Z=64) for $RETiNbO_6$, and Dy (Z=66) and Ho (Z=67) for $RETiTaO_6$. The principal difference between RE ions in these structures is that in aeschynites the RE ions lie in closely connected chains, whereas in euxenites they lie on densely packed parallel planes. The former usually exhibits a positive temperature coefficient of resonance frequency (τ_f) and a high permittivity (ε_r), whereas the latter presents a negative τ_f and a relatively low ε_r. $RETi(Nb,Ta)O_6$ ceramic materials with near-zero τ_f values were thus manufactured via synthesizing solid solutions between aeschynite and euxenite.[6]

Among these $RETi(Nb,Ta)O_6$ compounds, $LaTi(Nb,Ta)O_6$ belongs to a special one. It crystallizes into an O aeschynite structure at low temperatures, but transforms into a high-temperature monoclinic (M) aeschynite structure.[7] For $LaTiNbO_6$, the high-temperature M phase could

stably exist at room temperature, achieving good microwave dielectric properties of ε_r=22.3, $Q\times f$=49 867 GHz and τ_f=−55 ppm/°C.[8] By comparison, a single O-phase ceramic is difficult to attain at room temperature. The substitution of Ce or Sm at A-sites of $LaTiNbO_6$ was reported to induce an M–O phase transition, accompanying tunable microwave dielectric properties.[9] In addition, a single O-phase ceramic could be also achieved by an annealing process or by lowering the sintering temperature via Zn^{2+} substitution.[10,11] Actually, both M and O aeschynite consist of identical double-octahedron structure units $(Ti,Nb)_2O_{10}$, but these units connect in different ways, i.e. share edges in M structure and share corners in O structure.[12] Thereby, it could be speculated that M–O transition might be closely correlated with the variation in $(Ti,Nb)O_6$ octahedra in these structures. It would be of interest to explore how the B-site ionic substitution in $LaTiNbO_6$ could induce an M–O phase transition, and whether it played the same role as A-site RE ionic substitution did or not.

In this work, three typical isovalent cations (or compound ion) with different radii (coordination number is six),[13] such as larger cation Zr^{4+} (0.72 Å), equally sized Ta^{5+} (0.64 Å) and smaller $(W_{0.5}Ti_{0.5})^{5+}$ (0.6025 Å), were chosen to replace Ti^{4+} (0.605 Å) and Nb^{5+} (0.64 Å) of $LaTiNbO_6$, respectively. The crystal phase evolution, structure characteristics, microstructure, and microwave dielectric properties of equivalently substituted $LaTiNbO_6$ ceramics were investigated with a special focus on the influence of the variation in bond length and octahedral distortion on the phase structural stability and subsequent microwave dielectric properties.

2 | EXPERIMENTAL PROCEDURE

$LaTi_{1-x}Zr_xNbO_6$ (ZR-x, x=0-1), $LaTiNb_{1-y}Ta_yO_6$ (TA-y, y=0-1), $LaTiNb_{1-z}$ $(W_{0.5}Ti_{0.5})_zO_6$ (WT-z, z=0-1) ceramics were prepared by a routine solid-state reaction process. High-purity (>99%) La_2O_3, Nb_2O_5, TiO_2, ZrO_2, Ta_2O_5, and WO_3 powders were used as the starting materials. The raw powders of stoichiometric proportion were weighed and then ball milled using zirconia balls in ethanol medium for 4 hours. The resultant slurry was then dried and calcined at 1050°C-1150°C for 8 hours, followed by a second grinding process for 6 hours. The reground powders were mixed with 5 wt% PVA binders, and then pressed into cylinders with 10 mm in diameter and 5-6 mm in height under a uniaxial pressure of 200 MPa. The specimens were first heated at 550°C for 4 hours at 3°C/min to burn out the organic binder, and then sintered in the temperature range of 1250°C-1450°C for 4 hours at 5°C/min in ambient atmosphere.

The crystalline structures of the sintered samples were determined by an X-ray diffractometer (XRD, D/Max2500V, Rigaku, Tokyo, Japan) using CuK_α radiation. Prior to the examination, the sintered pellets were crushed into powders with a mortar. The diffraction patterns were obtained over a 2θ range of 10°-90° with a step of 0.02°. The XRD data were analyzed by the Rietveld refinement method using GSAS suite equipped with EXPGUI software.[14,15] The bulk densities of the sintered ceramics were measured using the Archimedes method. The theoretical density of the ceramics was obtained from the Rietveld refinement results. The microstructure of the sintered samples was observed using a field-emission scanning electron microscope (FE-SEM; SU8020, JEOL, Tokyo, Japan). A network analyzer (Agilent, N5230C, Palo Alto, CA) and a temperature chamber (GDW-100, Saiweisi, Changzhou, China) were used to measure the dielectric properties of the well-polished ceramic samples by means of a Hakki-Coleman post resonator method.[16,17] The τ_f values of the samples were measured in the temperature range from 20°C to 80°C. It can be calculated as follows:

$$\tau_f = \frac{f_2 - f_1}{f_1(T_2 - T_1)} \quad (1)$$

where f_1 and f_2 represent the resonant frequencies at T_1 and T_2, respectively.

3 | RESULTS AND DISCUSSION

In current work, $LaTiNbO_6$ ceramics could be well sintered at 1325°C, but ZR-x, TA-y, and WT-z ceramics at 1400°C, 1450°C and 1375°C, respectively. The XRD patterns of ZR-x, TA-y, and WT-z ceramics sintered at their optimum temperatures are given in Figure 1A-C, respectively. $LaTiNbO_6$ (x=0) was in the form of an M aeschynite structure with a *C2/c* space group as its peaks could be well indexed to the standard pattern of JCPDS files #15-0872. For ZR-x ceramics of Figure 1A, an obvious structure transformation from M to O could be observed as x=0.01-0.20. As can be clearly seen from the partially enlarged view in Figure 1D, O-typed $LaTiNbO_6$ appeared in a small amount among the M matrix at x=0.01, and then became dominant as $x\geq$0.03. As x=0.2, the M phase completely disappeared and a pure O phase was observed. With further increasing x, diffraction peaks of the O phase were found to slightly shift to low angles due to a larger radius of Zr^{4+} than Ti^{4+}. The above-mentioned phase structural evolution could be also reflected by the variation in the corresponding grain morphology, as shown in Figure 2. It can be seen that the x=0.01 and x=0.2 samples owned polygonal and short rod-like grain morphologies, respectively, which are

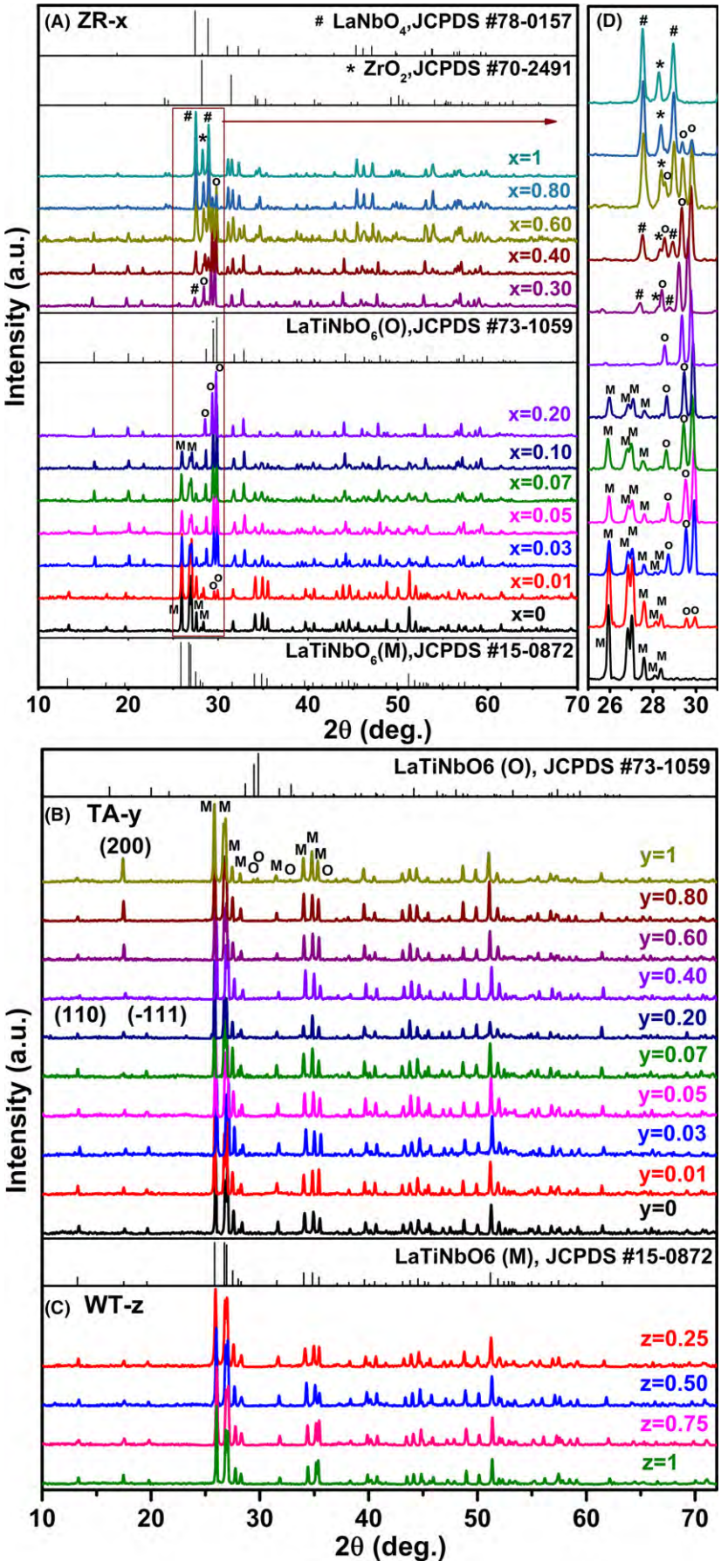

FIGURE 1 Normalized XRD patterns of (A) ZR-*x*, (B) TA-*y* and (C) WT-*z* ceramics sintered at their optimal temperatures, and (D) locally magnified view of diffraction line between 25° and 31° for ZR-*x* ceramics [Color figure can be viewed at wileyonlinelibrary.com]

typical of M and O-phase $LaTiNbO_6$ ceramics.[9-11,18] This observation well agreed with the XRD results in Figure 1A. For other samples with different x, the grain morphology displayed a typical feature of two-phase coexistence with bimodal grain morphology. Moreover, as $x>0.2$, $LaNbO_4$ and ZrO_2 secondary phases started to appear approximately at $x=0.3$, and became dominant as $x\geq0.60$. Finally, only $LaNbO_4$ and ZrO_2 were observed in the $x=1$ sample as their peaks matched well with the patterns of JCPDS files #78-0157 and #70-2491, respectively.

In contrast, an M-phase solid solution was formed almost in the whole composition range for TA-y and WT-z ceramics, as displayed in Figure 1B and C, apart from the $y=1$ sample in which a tiny amount of O phase (as marked as O) was observed. As shown in Figure 3, all compositions exhibited similar polygonal grain morphology to that of the undoped $LaTiNbO_6$ matrix, which is different from that observed in the ZR-x sample with $x=0.2$. Particularly for TA-y ceramics, larger grains (~40 μm) with some pores were observed in the TA-0.80 sample, as found in M-phase $LaTiTaO_6$ ceramics.[19] In addition, the intensity of (200) lines was found to increase with substituting Ta^{5+} for Nb^{5+}, and simultaneously the intensity of (110) and (−111) lines declined, especially as $y\geq0.60$. The same diffraction characteristic was reported in M-phase $LaTiTaO_6$ ceramics.[19] The (100) preferential orientation observed in $LaTiTaO_6$ or TA-y samples might account for the abnormal grain growth and some closed pores in these compositions, probably owing to the reduced energy for the grain boundary migration at a specific crystal plane. From the above-mentioned XRD and SEM results of TA-y and WT-z ceramics, an M–O phase structural transition at room temperature was not observed (except $y=1$) probably because of relatively small substitution ions compared to Nb^{5+} ions. That is to say, a larger cation at the B-site seems to be necessary for the stability of the O phase.

To further study the phase composition and crystal structure after B-site substitution, the XRD refinements of these samples were performed using GSAS software. The relative content of two coexisting phases in all different samples was identified by means of the multiphase Rietveld refinement of their XRD data. M-phase (ICDD# 413439)[12] and O-phase (ICDD# 23509)[20] $LaTiNbO_6$ were chosen as their initial modes, as presented in Table 1. The ion occupancy in the two models was revised according to the nominal composition before the refinement. As a representative, detailed structural parameters, reliability factors and goodness-of-fit indicator of ZR-x ceramics are listed in Table 2. The refinement reliable factors of R_{wp}, R_p, and χ^2 were found to be in the range of 7%-10%, 6%-8%, and 1.4-1.7, respectively, indicating that the structural model was valid and the refinement result was reliable. As can be seen from Table 2, the relative content of M and O phase decreased with increasing x. In addition, the lattice parameters and cell volumes of the O phase were found to increase with increasing x while they seemed not to change much for the M phase.

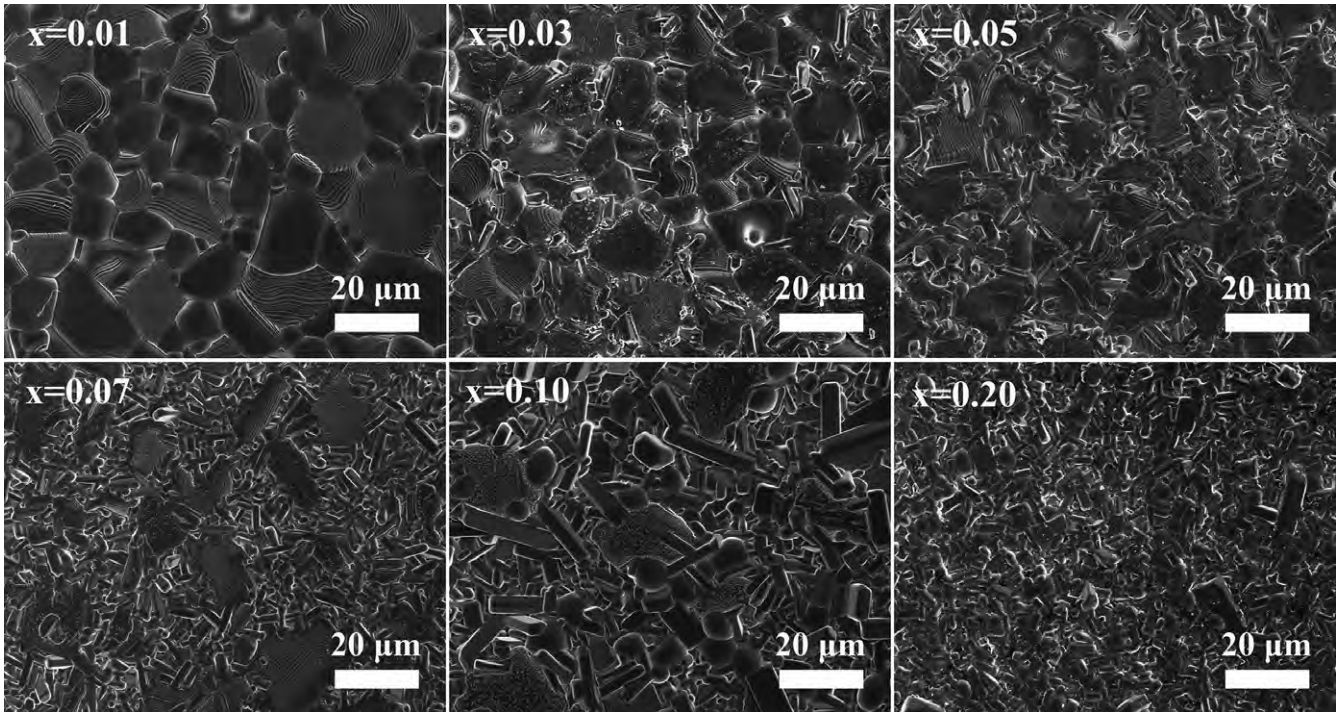

FIGURE 2 SEM micrographs of ZR-x (x=0.01-0.20) ceramics at 1400°C

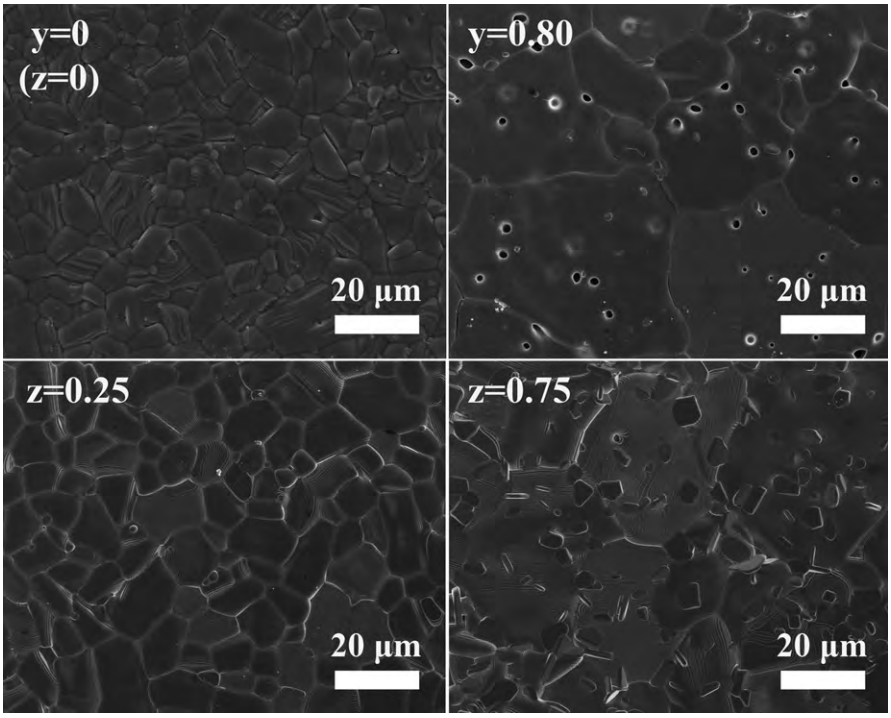

FIGURE 3 SEM images of TA-y and WT-z ceramics sintered at their optimal temperatures

According to the Ref. 21, the distortion of an octahedron (Δ) could be estimated as follows:

$$\Delta = \frac{1}{6}\sum\left(\frac{R_i - \overline{R}}{\overline{R}}\right)^2 \quad (2)$$

where R_i is the individual bond length, and $\overline{R}$ is the average bond length of oxygen octahedron. Δ could characterize the deviation of the octahedron in a crystal structure from a regular octahedron. It can be seen from the ion occupancy and bond information in $LaTiNbO_6$ in Table 1 that, there are three kinds of oxygen with six kinds of (Ti, Nb)–O bond in an M structure while four kinds of oxygen with six kinds of (Ti,Nb)–O bond in an O structure, as illustrated by sphere-rod graphs in Figure 4. It can be found in Table 1 that the average bond length at (Ti,Nb)-site was similar in M and O phases but the distortion of octahedron in the O structure was five times as large as that in the M structure. This suggests that Δ instead of $\overline{R}$ might be a crucial factor for the stability of O and M phases.

The variation in $\overline{R}$ and Δ in the M and O phase of ZR-x (x=0-0.20) ceramics is plotted in Figure 5. It can be observed from Figure 5A that the length of #1 and #4 bonds (as indicated in Figure 4) in the M phase slightly decreased as x increased up to 0.07 and then increased, but other four bonds slightly stretched with increasing x. In addition, the average bond length in octahedra of the M phase first remained stable and then increased as x>0.07 while the octahedral distortion decreased gradually. In contrast, all the six bonds in an octahedron of the O phase slightly stretched until x=0.10, and then remained stable up to the x=0.20 with a single-O structure. The octahedral distortion in O phase was slightly increased and then got stable gradually. The above results indicated that the octahedral bond length exhibited an anisotropic change for M phases but a uniform variation for O phases. Most importantly, the decrease in Δ values was found to be responsible for the destabilization of either O or M phases.

TABLE 1 Ion occupancy and bond information in two forms of $LaTiNbO_6$

$LaTiNbO_6$ (M)[12]			$LaTiNbO_6$ (O)[20]		
Ion	**Wyckoff site**	**Occ.**	**Ion**	**Wyckoff site**	**Occ.**
La	4e	1	La	4c	1
Nb	8f	0.5	Nb	8d	0.5
Ti	8f	0.5	Ti	8d	0.5
O1	8f	1	O1	8d	1
O2	8f	1	O2	8d	1
O3	8f	1	O3	4c	1
—	—	—	O4	4c	1
Bond in octahedra	Nb/Ti–O1 (#1): 1.987 Å Nb/Ti–O1 (#3): 1.951 Å Nb/Ti–O2 (#5): 1.925 Å Nb/Ti–O2 (#6): 2.048 Å Nb/Ti–O3 (#2): 2.011 Å Nb/Ti–O3 (#4): 2.014 Å $\overline{R}_M$: 1.9893 Å Δ_M: 4.268×10^{-4}			Nb/Ti–O1 (#5): 1.947 Å Nb/Ti–O1 (#6): 2.157 Å Nb/Ti–O2 (#2): 2.020 Å Nb/Ti–O2 (#3): 1.852 Å Nb/Ti–O3 (#4): 1.959 Å Nb/Ti–O4 (#1): 1.922 Å $\overline{R}_O$: 1.9762 Å Δ_O: 2.310×10^{-3}	

TABLE 2 Rietveld refinement results of ZR-x (x=0-0.20) ceramics

x	0	0.01	0.03	0.05	0.10	0.20
M (wt%)	100	92.6 (7)	39.7 (3)	32.4 (5)	31.9 (5)	0
O (wt%)	0	7.4 (5)	60.3 (2)	67.6 (2)	68.1 (3)	100
M phase						
a (Å)	11.195 (2)	11.1903 (7)	11.194 (1)	11.190 (2)	11.194 (2)	—
b (Å)	8.842 (2)	8.8420 (6)	8.8437 (9)	8.844 (1)	8.857 (2)	—
c (Å)	5.268 (1)	5.2657 (4)	5.2682 (6)	5.2659 (9)	5.264 (1)	—
α=β (°)	90	90	90	90	90	—
γ (°)	115.332 (3)	115.308 (3)	115.362 (6)	115.363 (9)	115.29 (1)	—
V (Å^3)	471.4 (3)	471.01 (6)	471.29 (7)	470.9 (1)	471.9 (1)	—
O phase						
a (Å)	—	10.938 (3)	10.9446 (6)	10.949 (1)	10.9980 (9)	11.007 (2)
b (Å)	—	7.583 (2)	7.5821 (4)	7.5836 (6)	7.6046 (5)	7.608 (1)
c (Å)	—	5.437 (2)	5.4459 (3)	5.4460 (5)	5.4577 (4)	5.4597 (8)
α=β=γ (°)	—	90	90	90	90	90
V (Å^3)	—	451.0 (2)	451.92 (6)	452.23 (9)	456.46 (8)	457.2 (2)
R_{wp} (%)	9.71	8.51	7.87	8.79	8.76	8.45
R_p (%)	7.64	6.66	6.21	6.98	6.88	6.68
χ^2 (%)	1.498	1.61	1.503	1.594	1.619	1.674

The $\overline{R}$ and Δ values of the M-phase octahedra in ZR-x, TA-y, and WT-z ceramics as well as in A-site substituted $LaTiNbO_6$ ceramics ($La_{1-p}Ce_pTiNbO_6$ (CE-p, p=0-0.2) and $La_{1-q}Sm_qTiNbO_6$ (SM-q, q=0-0.15))[9] are shown in Figure 6. It can be seen that, the $\overline{R}$ value increased when more and larger cations were introduced, and decreased for more and smaller substitution cations, irrespective of A-site or B-site substitution, as can be seen from Figure 6A. By comparison, the Δ value did not have a straightforward relation with the radius of substitution ions. The substitution of either smaller Ce^{3+} and Sm^{3+} ions or larger Zr^{4+} ions were found to cause the decrease in the Δ value of M phase, as can be seen from Figure 6B. Moreover, the substitution of smaller $(W_{0.5}Ti_{0.5})^{5+}$ ions can lead to the increase in the Δ value of M phase. Nevertheless, considering the variation in the room-temperature phase structures in A-site or B-site substituted $LaTiNbO_6$ ceramics (see Figure 1 and Ref. 9), the Δ value and the phase structural stability were found to be more strongly correlated. That is to say, the octahedral distortion instead of the average bond length and substitution ionic radius would decisively influence the phase structural stability of O and M phases. Clearly, the ionic substitution that leads to the reduction in octahedral distortion would promote the M to O phase transition.

Microwave dielectric properties of ZR-x ceramics are presented in Figure 7. It can be seen that ε_r increased from 22.5 to 56 and τ_f changed from −54 to 85 ppm/°C as x increased up to 0.2, in which the variation in both ε_r and τ_f values generally conformed to the two-phase mixing rule and also exhibited a synchronous change, as commonly observed in some microwave dielectric ceramics.[22,23] $Q\times f$ values also decreased with x in this composition range owing to the appearance of the high-loss O phase. A near-zero τ_f value as well as ε_r=28.2 and $Q\times f$=25 113 GHz (6.75 GHz) was yielded as x=0.028 in which O and M phases coexisted. The ZR-0.20 sample with a single O phase exhibited microwave dielectric properties of ε_r=56.2, $Q\times f$=7382 GHz (4.88 GHz) and τ_f=85.4 ppm/°C. For comparison, dielectric properties of O-phase $LaTiNbO_6$ ceramics prepared in different ways are listed in Table 3. In addition to the annealed sample, all other samples owned a relatively high density. That is to say, the property difference of these samples might primarily depend on the intrinsic factors, in which the theoretical ionic polarizability ($\alpha_{theo.}$) was calculated using the additivity rule.[24] It can be found that ε_r of the Zr-substituted sample was slightly larger than that of the Sm-substituted one but smaller than that of Zn- and Ce-substituted ones, which might be ascribed to the competition between the positive effect of the largest $\alpha_{theo.}$ value and the negative effect of the largest volume, according to the Clausius–Mosotti equation.[24] Particularly, the lowest $Q\times f$ value was observed in the Zr-substituted sample probably owing to the reduced packing fraction (PF) caused by the substitution of larger cations, similar to that observed in spinel.[25] As PF increased, the intrinsic loss decreased due to weakened lattice vibrations, leading to improved

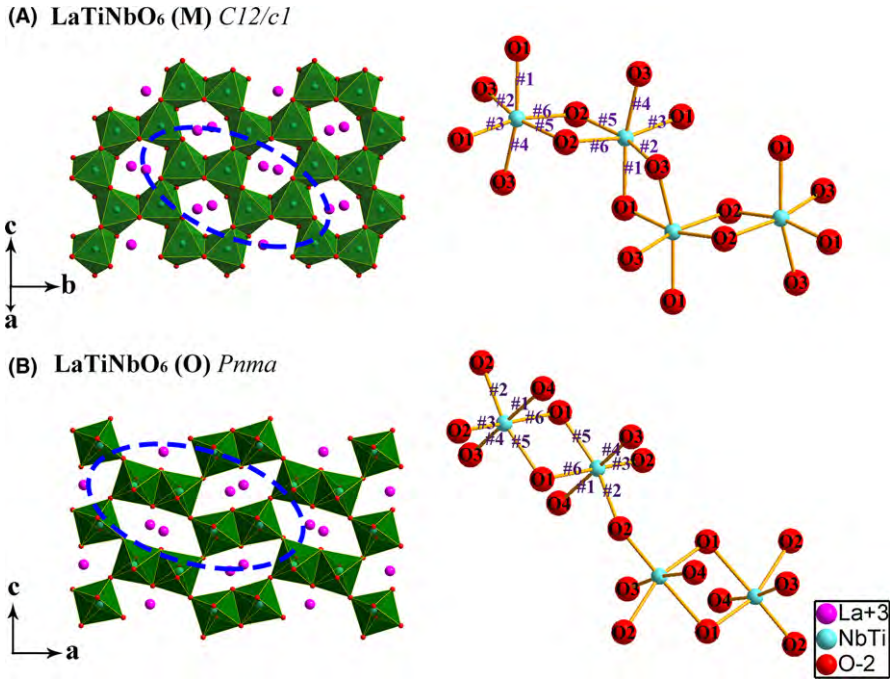

FIGURE 4 Schematic diagrams of the crystal structure and double-octahedron unit in (A) M- and (B) O-typed $LaTiNbO_6$ [Color figure can be viewed at wileyonlinelibrary.com]

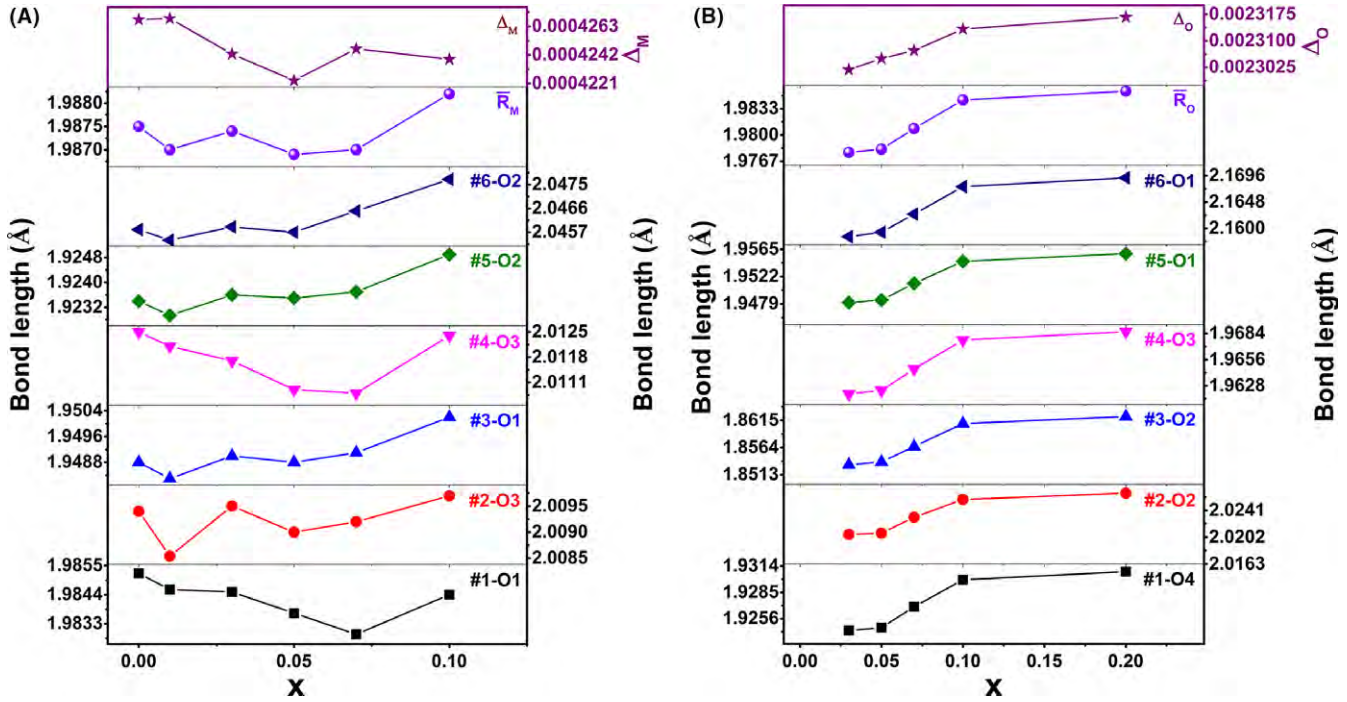

FIGURE 5 Variation in bond length and distortion in octahedra of the (A) M and (B) O phases in ZR-x ceramics [Color figure can be viewed at wileyonlinelibrary.com]

$Q\times f$ values.[26] With further increasing x above 0.2 in ZR-x ceramics, the reduced ε_r and τ_f values along with a slightly increased $Q\times f$ value were believed to be a result of the secondary phase $LaNbO_4$ (ε_r=19.3, $Q\times f$=54 400 GHz, and τ_f=9 ppm/°C).[27]

In addition, microwave dielectric properties of TA-y and WT-z ceramics are listed in Table 4. As y was beyond 0.60, a rapid decrease in ε_r and $Q\times f$ occurred. This might be due to the reduced density (Figure 3B) and residual high-loss O phase (Figure 1B). In contrast, WT-z ceramics presented similar changes with z in ε_r and $Q\times f$ while τ_f increased monotonously as a result of the increased octahedral distortion, as shown in Figure 6B, which agreed well with previous work.[28] It was known that τ_f is inversely

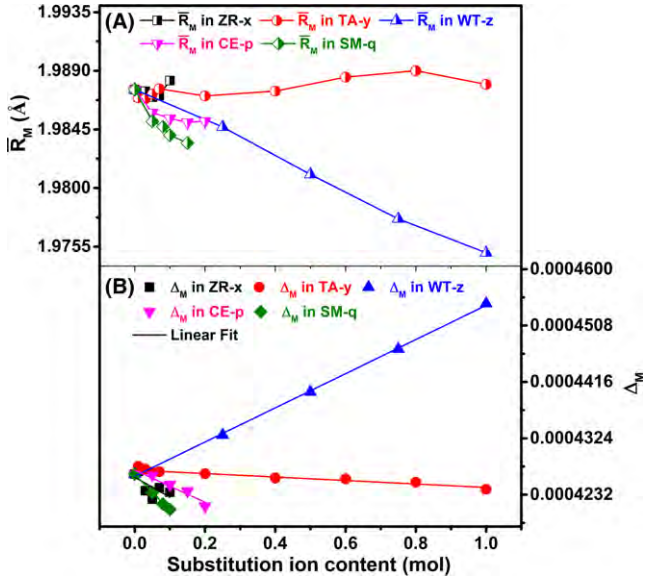

FIGURE 6 (A) The average bond length and (B) the distortion of M-phase octahedra in ZR-*x*, TA-*y*, WT-*z*, CE-*p* and SM-*q* ceramics as indicated [Color figure can be viewed at wileyonlinelibrary.com]

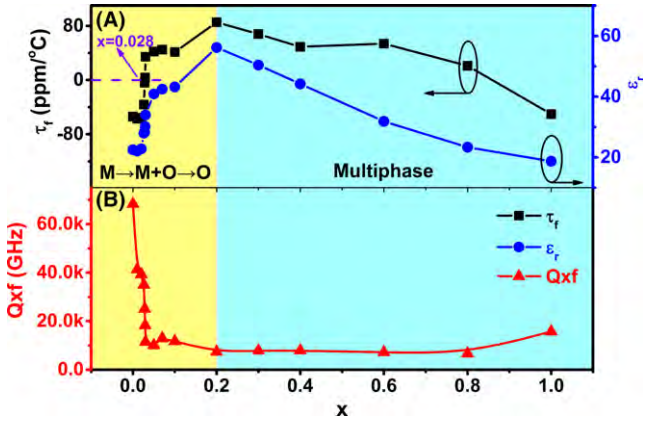

FIGURE 7 Microwave dielectric properties of ZR-*x* ceramics sintered at their optimal temperatures [Color figure can be viewed at wileyonlinelibrary.com]

proportional to the polarizability of the compounds, however, the latter is inversely proportional to the restoring force between respective ions in compounds.[29] The substitution of $(W_{0.5}Ti_{0.5})^{5+}$ ions increased the octahedral distortion (see Figure 6B) and thus increased the restoring forces between cations and anions so that τ_f increased.[28-30] In general, in case of TA-*y* and WT-*z* ceramics, their microwave dielectric properties exhibited a monotonous relationship with the substitution ion content, because no phase structural transition was involved. Besides, it was also found that totally different microwave dielectric properties were observed in M-phase TA-0.20 and WT-0.25 samples compared with the O-phase samples such as ZR-0.2, as shown in Table 3. This indicated that the dielectric performance of aeschynite ceramics mainly depended on the phase structure rather than compositions. The higher ε_r of the O phase should be mainly related with its smaller unit cell volume in consideration of their similar $\alpha_{theo.}$ values in both phase structures. Completely opposite-sign τ_f values between O and M phases essentially originated from

TABLE 4 Microwave dielectric properties of TA-*y* and WT-*z* ceramics sintered at their optimal temperatures

	ρ (%)	ε_r	$Q\times f$ (GHz)	f (GHz)	τ_f (ppm/°C)
TA-*y*					
0	94.4	22.5	68 258	7.49	−54
0.01	96.0	22.5	93 818	7.37	−60
0.03	96.3	23.0	94 839	7.37	−54.4
0.05	96.0	22.9	72 039	7.36	−62.3
0.07	95.2	22.5	71 257	7.40	−55.1
0.20	96.5	21.0	96 978	7.63	−64.1
0.40	95.5	20.4	98 162	7.76	−61.5
0.60	94.5	20.2	106 582	7.79	−66.5
0.80	73.8	15.7	49 907	8.29	−56.6
1	81.9	17.7	34 790	8.03	−50.4
WT-*z*					
0.25	96.3	22.6	88 254	7.39	−56.1
0.5	96.3	21.4	81 312	7.55	−67.9
0.75	94.4	20.4	72 444	7.72	−75.8
1	95.4	20.4	65 889	7.83	−72.7

TABLE 3 Microwave dielectric properties of aeschynite $LaTiNbO_6$ ceramics prepared via different methods

Composition	S. T. (°C)	Phase	ρ (%)	$\alpha_{theo.}$	V (Å^3)	PF (%)	ε_r	$Q\times f$ (GHz)	f (GHz)	τ_f (ppm/°C)	Ref.
Annealed $LaTiNbO_6$	—	O	90.1	25.03	451.32 (4)	68.68	48.7	10 018	5.21	69.7	10
$La_{0.97}Zn_{0.03}TiNbO_{5.985}$	1200	O	98.0	24.91	451.5 (2)	68.56	62.4	9671	4.77	105.5	11
$La_{0.7}Ce_{0.3}TiNbO_6$	1350	O	99.1	25.05	449.8 (2)	68.83	63.4	13 652	4.56	111.2	9
$La_{0.8}Sm_{0.2}TiNbO_6$	1400	O	98.3	24.76	446.85 (9)	69.14	52.6	15 101	5.09	86.9	9
ZR-0.20	1400	O	99.2	25.09	457.2 (2)	67.91	56.2	7382	4.88	85.4	This work
TA-0.20	1450	M	96.5	25.18	471.0 (3)	65.81	21.0	96 978	7.63	−64.1	This work
WT-0.25	1375	M	96.3	24.80	469.4 (5)	65.99	22.6	88 254	7.39	−56.1	This work

S.T., sintering temperature; ρ, relative density; PF, packing fraction; $\alpha_{theo.}$, theoretical polarizability; Ref, references.

their own structure-chemical characteristics, especially the tilting of $(Ti,Nb)O_6$ octahedra.[31] The octahedra in O phase with corner-sharing double-octahedron units were more likely to tilt than that in M phase, where double-octahedron units shared edges,[10,32] as displayed in Figure 4. In addition, the O-phase ceramic was found to present a much smaller $Q\times f$ but a larger PF value, which also went against the general knowledge. Actually, $Q\times f$ should be influenced by a few parameters such as sample density, impurity, secondary phase, grain size, etc. In current work, a large dielectric loss in the O-phase ceramic might be ascribed to its massive grain boundary effect from ten times smaller grains than that in the M-phase ceramic, as shown in Figures 2 and 3. The grain boundary can be as a main contributor to the dielectric loss, because it is prone to act as a sink for impurities and defects.[33]

4 | CONCLUSIONS

The phase composition, grain morphology and microwave dielectric properties of equivalently substituted $LaTiNbO_6$ ceramics were found to evolve with the site occupancy and radius of the substitution ions. Accompanied by a transition of grain morphology from polygonal to short rod-like ones, an M–O phase structural transition appeared in ZR-x ceramics as well as in CE-p and SM-q ceramics, while a single M phase was obtained almost in the whole composition of TA-y, and WT-z ceramics with a nearly unchanged grain morphology. The Rietveld structural refinement of XRD data suggested that a more straightforward relation should be built up between the phase stability of O or M aeschynites and the octahedral distortion instead of the octahedral average bond length. Irrespective of the substitution ionic radius and occupancy, the reduction in octahedral distortion was believed to be responsible for the destabilization of O or M phases. A near-zero τ_f value as well as ε_r=28.2 and $Q\times f$=25 113 GHz (6.75 GHz) was yielded as x=0.028 in which O and M phases coexisted. The ZR-0.20 sample with a single O phase exhibited microwave dielectric properties of ε_r=56.2, $Q\times f$=7382 GHz (4.88 GHz) and τ_f=85.4 ppm/°C. However, the TA-0.2 or WT-0.25 sample with a single M phase owned dielectric properties of ε_r=~21, $Q\times f$=~90 000 GHz (7.50 GHz) and τ_f=~−60 ppm/°C on average. Totally different microwave dielectric performances between two types of aeschynites were believed to basically originate from their distinct phase structure and grain morphology.

ACKNOWLEDGMENTS

This work was financially supported by the Special Funds for Science and Technology Development of Guangdong Province (Grant No. 2017A010101001) and the Natural Science Foundation of Anhui Province (Grant No. 1508085JGD04).

REFERENCES

1. Qi X, Han TPJ, Gallagher HG, et al. Optical spectroscopy of $PrTiNbO_6$, $NdTiNbO_6$ and $ErTiNbO_6$ single crystals. *J Phys Condens Matter*. 1996;8:4837-4846.
2. Qi X, Illingworth R, Gallagher HG, et al. Potential laser gain media with the stoichiometric formula $RETiNbO_6$. *J Cryst Growth*. 1996;160:111-118.
3. Qi X, Liu CM, Kuo CC. Pr^{3+} doped $LaTiNbO_6$ as a single phosphor for white LEDs. *J Alloys Compd*. 2010;492:L61-L63.
4. Sebastian MT, Solomon S, Ratheesh R, et al. Preparation, characterization, and microwave properties of $RETiNbO_6$ (RE = Ce, Pr, Nd, Sm, Eu, Gd, Tb, Dy, Y, and Yb) dielectric ceramics. *J Am Ceram Soc*. 2001;84:1487-1489.
5. Surendran KP, Solomon S, Varma MR, et al. Microwave dielectric properties of $RETiTaO_6$ (RE = La, Ce, Pr, Nd, Sm, Eu, Gd, Tb, Dy, Ho, Y, Er, Yb, Al, and In) ceramics. *J Mater Res*. 2002;17:2561-2566.
6. Surendran KP, Varma MR, Mohanan P, et al. Microwave dielectric properties of $RE_{1-x}RE'_xTiNbO_6$ [RE = Pr, Nd, Sm; RE′ = Gd, Dy, Y] ceramics. *J Am Ceram Soc*. 2003;86:1695-1699.
7. Strakhov VI, Mel'nikova OV, Dib M. Phase diagram for the system $LaNbO_4$–TiO_2. *Inorg Mater* 1991;27:495-498.
8. Bian JJ, Li YZ, Yuan LL. Structural stability and microwave dielectric properties of $(1-x)Ln_{1/3}NbO_3$–$xLn_{2/3}TiO_3$ (Ln: La, Nd; $0\le x\le 0.8$). *Mater Chem Phys*. 2009;116:102-106.
9. Zhang J, Zuo RZ. Phase structural transition and microwave dielectric properties in isovalently substituted $La_{1-x}Ln_xTiNbO_6$ (Ln = Ce, Sm) ceramics. *Ceram Int*. 2017;43:7065-7072.
10. Zhang J, Zuo RZ. A novel self-composite property-tunable $LaTiNbO_6$ microwave dielectric ceramic. *Mater Res Bull*. 2016;83:568-572.
11. Zhang J, Zuo RZ. Sintering behavior, structural phase transition and microwave dielectric properties of $La_{1-x}Zn_xTiNbO_{6-x/2}$ ceramics. *J Am Ceram Soc*. 2017;. https://doi.org/10.1111/jace.14934.
12. Golobič A, Škapin SD, Suvorov D, et al. Solving structural problems of ceramic materials. *Croat Chem Acta*. 2004;77:435-446.
13. Shannon RD. Revised effective ionic radii and systematic studies of interatomic distances in halides and chalcogenides. *Acta Cryst A*. 1976;32:751-767.
14. Larson AC, Von Dreele RB. *General Structural Analysis System (GSAS)*. New Mexico: Los Alamos National Laboratory Report LAUR; 2000.
15. Toby BH. EXPGUI, a graphical user interface for GSAS. *J Appl Crystallogr*. 2001;34:210-213.
16. Hakki BW, Coleman PD. A dielectric resonant method of measuring inductive capacities in the millimeter range. *IEEE Trans Microwave Theory Tech*. 1960;8:402-410.
17. Courtney WE. Analysis and evaluation of a method of measuring the complex permittivity and permeability of microwave insulators. *IEEE Trans Microwave Theory Tech*. 1970;18:476-485.
18. Oishi T, Kan A, Ohsato H, et al. Crystal structure–microwave dielectric property relations in $Sm(Nb_{1-x}Ta_x)(Ti_{1-y}Zr_y)O_6$ ceramics. *J Eur Ceram Soc*. 2006;26:2075-2079.
19. Kasunič M, Škapin SD, Suvorov D, et al. Polymorphism of $LaTaTiO_6$. *Acta Chim Slov*. 2012;59:117-123.

20. Fauquier D, Gasperin M. Synthesis of monocrystals and structural study of $LaNbTiO_6$. *Bull Soc Fran Min Crist*. 1970;93:258-259.
21. Kim ES, Choi W. Effect of phase transition on the microwave dielectric properties of $BiNbO_4$. *J Eur Ceram Soc*. 2006;26:1761-1766.
22. Sebastian MT, Ubic R, Jantunen H. Low-loss dielectric ceramic materials and their properties. *Int Mater Rev*. 2015;60:392-412.
23. Sebastian MT, Wang H, Jantunen H. Low temperature co-fired ceramics with ultra-low sintering temperature: a review. *Curr Opin Solid State Mater Sci*. 2016;20:151-170.
24. Shannon RD. Dielectric polarizabilities of ions in oxides and fluorides. *J Appl Phys*. 1993;73:348-366.
25. Zhang J, Zuo RZ. Effect of ordering on the microwave dielectric properties of spinel-structured $(Zn_{1-x}(Li_{2/3}Ti_{1/3})_x)_2TiO_4$ ceramics. *J Am Ceram Soc*. 2016;99:3343-3349.
26. Kim ES, Chun BS, Freer R, et al. Effects of packing fraction and bond valence on microwave dielectric properties of $A^{2+}B^{6+}O_4$ (A^{2+}: Ca, Pb, Ba; B^{6+}: Mo, W) ceramics. *J Eur Ceram Soc*. 2010;30:1731-1736.
27. Kim DW, Kwon DK, Yoon SH, et al. Microwave dielectric properties of rare-earth ortho-niobates with ferroelasticity. *J Am Ceram Soc*. 2006;89:3861-3864.
28. Ramarao SD, Murthy VRK. Crystal structure refinement and microwave dielectric properties of new low dielectric loss $AZrNb_2O_8$ (A: Mn, Zn, Mg and Co) ceramics. *Scripta Mater*. 2013;69:274-277.
29. Lee HJ, Hong KS, Kim SJ, et al. Dielectric properties of MNb_2O_6 compounds (where M = Ca, Mn Co, Ni, or Zn). *Mater Res Bull*. 1997;32:847-855.
30. Kim ES, Jeon CJ, Kim SJ, et al. Effects of crystal structure on microwave dielectric properties of ceramics. *J Koren Ceram Soc*. 2008;45:251-255.
31. Colla EL, Reaney IM, Setter N. A microscopic model for the temperature coefficient of the resonant frequency (τ_f) in complex perovskites used for microwave filter. *Ferroelectrics*. 1994;154:35-40.
32. Megaw HD. Crystal structures and thermal expansion. *Mater Res Bull*. 1971;6:1007-1018.
33. Breeze JD, Perkins JM, McComb DW, et al. Do grain boundaries affect microwave dielectric loss in oxides. *J Am Ceram Soc*. 2009;92:671-674.

How to cite this article: Zhang J, Zuo R. Octahedral distortion, phase structural stability, and microwave dielectric properties in equivalently substituted $LaTiNbO_6$ ceramics. *J Am Ceram Soc*. 2017;100:5249–5258. https://doi.org/10.1111/jace.15077